Synapsin Condensation is Governed by Sequence-Encoded Molecular Grammars ☆

Christian Hoffmann [1,†], Kiersten M. Ruff [2,†], Irina A. Edu [3], Min Kyung Shinn [2], Johannes V. Tromm [1], Matthew R. King [2], Avnika Pant [2], Hannes Ausserwöger [3], Jennifer R. Morgan [4], Tuomas P. J. Knowles [3,5], Rohit V. Pappu [2,*], and Dragomir Milovanovic [1,6,7,8,*]

*1 - **Laboratory of Molecular Neuroscience Berlin,** German Center for Neurodegenerative Diseases (DZNE), 10117 Berlin, Germany*
*2 - **Department of Biomedical Engineering and Center for Biomolecular Condensates,** James McKelvey School of Engineering, Washington University in St. Louis, St. Louis, MO, USA*
*3 - **Centre for Misfolding Diseases,** Yusuf Hamied Department of Chemistry, University of Cambridge, Lensfield Road, Cambridge CB2 1EW, United Kingdom*
*4 - **Eugene Bell Center for Regenerative Biology and Tissue Engineering,** Marine Biological Laboratory, Woods Hole, MA 02543, USA*
*5 - **Cavendish Laboratory,** Department of Physics, University of Cambridge, JJ Thomson Road, Cambridge CB3 0HE, United Kingdom*
*6 - **German Center for Neurodegenerative Diseases (DZNE),** 53127 Bonn, Germany*
*7 - **Einstein Center for Neuroscience,** Charité-Universitätsmedizin Berlin, Corporate Member of Freie Universität Berlin, Humboldt-Universität Berlin, and Berlin Institute of Health, 10117 Berlin, Germany*
*8 - **Whitman Center,** Marine Biological Laboratory, 02543 Woods Hole, MA, USA*

Correspondence to Rohit V. Pappu and Dragomir Milovanovic: Laboratory of Molecular Neuroscience Berlin, German Center for Neurodegenerative Diseases (DZNE), 10117 Berlin Germany and Department of Biomolecular Engineering and Center for Biomolecular Condensates, James McKelvey School of Engineering, Washington University in St. Louis, St. Louis, MO, USA. *pappu@wustl.edu (R.V. Pappu), dragomir.milovanovic@dzne.de (D. Milovanovic)*
https://doi.org/10.1016/j.jmb.2025.168987
Editor: Garfinkle Shana Elabum

Abstract

Multiple biomolecular condensates coexist at the pre- and post- synapse to enable vesicle dynamics and controlled neurotransmitter release in the brain. In pre-synapses, intrinsically disordered regions (IDRs) of synaptic proteins are drivers of condensation that enable clustering of synaptic vesicles (SVs). Using computational analysis, we show that the IDRs of SV proteins feature evolutionarily conserved non-random compositional biases and sequence patterns. Synapsin-1 is essential for condensation of SVs, and its C-terminal IDR has been shown to be a key driver of condensation. Focusing on this IDR, we dissected the contributions of two conserved features namely the segregation of polar and proline residues along the linear sequence, and the compositional preference for arginine over lysine. Scrambling the blocks of polar and proline residues weakens the driving forces for forming micron-scale condensates. However, the extent of clustering in subsaturated solutions remains equivalent to that of the wild-type synapsin-1. In contrast, substituting arginine with lysine significantly weakens both the driving forces for condensation and the extent of clustering in subsaturated solutions. Co-expression of the scrambled variant of synapsin-1 with synaptophysin results in a gain-of-function phenotype in cells, whereas arginine to lysine

☆ This article is part of a special issue entitled: 'Biomolecular Condensates (2025)' published in Journal of Molecular Biology.

substitutions eliminate condensation in cells. We report an emergent consequence of synapsin-1 condensation, which is the generation of interphase pH gradients that is realized via differential partitioning of protons between coexisting phases. This pH gradient is likely to be directly relevant for vesicular ATPase functions and the loading of neurotransmitters. Our studies highlight how conserved IDR grammars serve as drivers of synapsin-1 condensation.

Introduction

Functional neurotransmission relies on repeated cycles of synaptic vesicle (SV) exocytosis and endocytosis at the synapse. As part of this cycle, hundreds of SVs are clustered at the pre-synapse, forming distinct biomolecular condensates driven by highly abundant synaptic proteins including synapsins.[1–3] Synapsin-SV condensates enable reversible sequestration and maintenance of soluble synaptic proteins that are essential for distinct steps of SV cycles.[4,5] Pre-synapses appear to be complex emulsions defined by multiple coexisting phases composed of synapsins, synaptophysin, synucleins, and other pre-synaptic proteins.[5]

The C-terminal intrinsically disordered region (IDR) in synapsin-1 is required for driving phase separation in cells and *in vitro*.[1] Additionally, antibody binding to this IDR disperses SV clusters at lamprey synapses.[2] In cells, co-expression of synapsin-1 with synaptophysin (SYP), a resident SV membrane protein, is required for condensation.[6] Interactions between the cytosolic tail of SYP and the C-terminal IDR of synapsin-1 drive condensation.[6] The working hypothesis is that complementary electrostatic interactions contribute to co-condensation of SYP and synapsin-1.[6–8] The synapsin-1 IDR can also interact with SH3 domain-containing proteins, including intersectin, to drive condensation *in vitro* and regulate nanoscale organization in cells.[1,9] Taken together, the extant data suggest that both IDR-IDR and IDR-structured domain interactions are important for the formation and regulation of synapsin-SV condensates.

Here, we report that pre-synaptic proteins feature IDRs defined by distinct molecular grammars. Molecular grammars refer to the non-random compositional biases and binary sequence patterns within an IDR.[10–14] Our computational analysis is suggestive of the molecular grammars within IDRs of SV proteins enabling complementary interactions among IDRs that make up SVs. Mutations to the synapsin-1 IDR that perturb its molecular grammars can abolish SV condensation *in vitro* and in cells. Using microfluidics-based scanning to measure phase boundaries and microfluidic resistive pulse sensing (MRPS) to quantify size distributions of clusters in subsaturated solutions,[15,16] we characterized the differential effects of molecular grammars on the assembly of synapsin-1 condensates. This helps show how certain features such as amino acid composition affect both clustering and phase separation, whereas other features such as sequence patterning, without changes to compositions, affect phase separation but do not affect clustering. Finally, using pH-sensitive fluorescence dyes, we demonstrate that protons partition preferentially into dense phases of synapsin-1 condensates, thus generating a distinct chemical environment.

Results

IDRs of SV proteins are defined by distinct and complementary molecular grammars

Previous studies have shown that IDRs of proteins that make up condensates are defined by condensate-specific molecular grammars.[10,17–23] We find that approximately 50% of resident SV proteins[22] and SV-accessory proteins[23] contain IDRs. To assess if distinct molecular grammars exist within the IDRs of resident SV proteins and soluble SV-accessory proteins, we deployed NARDINI+, which calculates the z-scores of 90 sequence features for each SV protein.[11,12,19,23]

The z-scores carry specific interpretations: If the feature in question quantifies a compositional bias, then the z-score quantifies the extent to which the feature is enriched or depleted when compared to the human IDRome. Positive z-scores signify enrichment, whereas negative z-scores signify depletion. If the feature in question is the degree of mixing or segregation of a pair of residue types, then a positive z-score implies a linear sequence segregation of the residue types, whereas a negative z-score implies that the residue types are well-mixed in the linear sequence. The magnitudes of these patterning z-scores quantify the extent of non-random segregation or mixing and this is calibrated against an ensemble of randomly shuffled sequences, where the composition is identical to the sequence of interest.[12] The 90 features that were analyzed for each sequence quantify compositional biases and non-random patterning.

We find that IDR grammars of resident SV proteins and accessory proteins are distinct from one another and IDRs of proteins that belong to other condensates (Figure 1A). Compositionally,

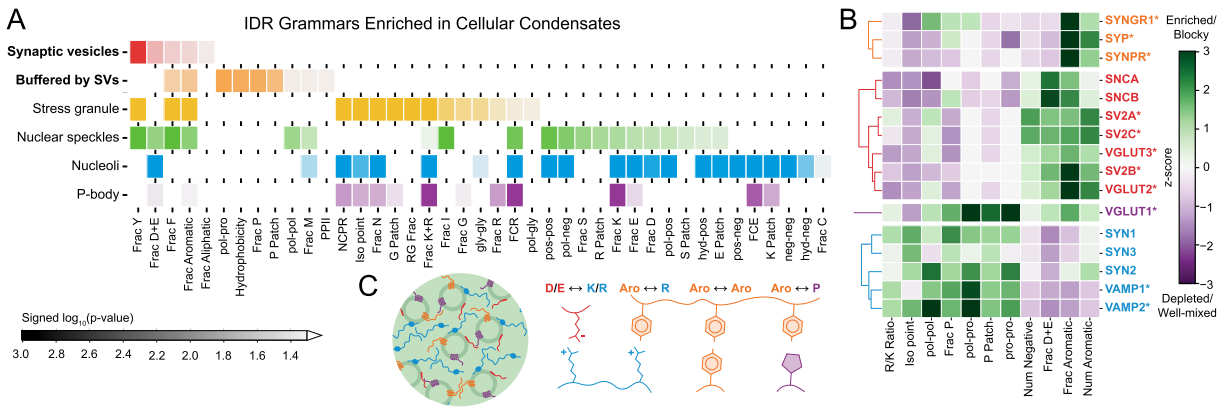

Figure 1. IDRs of proteins that make up synaptic condensates feature distinct molecular grammars. A. NARDINI+ analysis shows that IDR grammars of SV proteins are distinct from those of IDRs in other condensates. *P*-values were calculated using the two-sample Kolmogorov-Smirnov test between the distribution of *z*-scores for IDRs in each condensate versus the distribution of z-scores for all remaining IDRs of length $\geq$ 30 in the human proteome **B.** NARDINI+ analysis of main SV proteins. Compositions and sequence patterns of IDRs of pre-synaptic proteins fall into distinct clusters denoted by dendrograms and different colors of the protein names. Here, * denotes SV resident proteins. **C.** Schematic illustrating the chemical complementarity across IDRs within proteins that are a part of SV clusters.

IDRs of resident SV proteins are enriched in negatively charged and aromatic residues when compared to the human IDRome (Figure 1A). Archetypes of these IDRs include the cytoplasmic tails of SYP and synaptogyrin-1 (SYNGR1), which are enriched in aromatic residues, and the cytoplasmic tails of the vesicular glutamate transporters (VGLUTs) and the synaptic vesicle glycoproteins (SV2s) which are enriched in both negatively charged and aromatic residues (Figure 1B). In contrast, soluble SV-accessory proteins are enriched in proline and blocks of polar and proline residues that are non-randomly segregated from one another along the linear sequence (Figure 1A). Additionally, many of the IDRs in the SV proteins are positively charged with a clear preference for arginine over lysine residues, and this includes the synapsins (SYNs) (Figure 1B).

The molecular grammars of IDRs in resident transmembrane and accessory SV proteins are conserved across metazoans from lampreys, the oldest vertebrate predecessor, to humans (SI Appendix Figure S1). The distinct IDR grammars enriched in the resident and accessory SV proteins are suggestive of chemical complementarity that likely mediates the formation and regulation of SV condensates. Chemical complementarity is important for driving of homotypic (between pairs of the same IDR) and heterotypic (between different pairs of IDRs) interactions. Signature of chemical complementarity include the presence of: oppositely charged residues, aromatic residues, proline and aromatic residues, as well as cationic and pi residues, especially arginine and aromatic residues (Figure 1C).[8,24]

In cell and in vitro assessments of the effects of distinct molecular grammars

To assess the impact of distinct molecular grammars on SV condensation, we focused on synapsin-1, which is a key protein that drives the assembly of SV condensates.[1] Synapsin-1 has an N-terminal IDR, a substrate binding domain, and a C-terminal IDR (SI Appendix Figure S2A). The C-terminal IDR is enriched in blocks of polar and proline residues that are segregated from one another. This IDR also shows a clear preference for arginine over lysine (Figure 2).

To test the impacts of these distinctive grammars on synapsin-1 phase separation, we designed two variants of synapsin-1 where the designs focused on the C-terminal IDR. In the SCR variant, we scrambled the sequence of the IDR to disrupt proline/polar blocks while keeping the overall amino acid composition fixed (Figures 2, 3A, SI Appendix Figure S2B). In the RtoK variant, arginine residues within the IDR were substituted with lysine (Figures 2, 3B, SI Appendix Figure S2B). This mutant was designed to alter the chemical complementarity while maintaining the basic nature of the residues and their patterning within the sequence.

In cells, co-expression of SYP is necessary for synapsin-1 condensation.[6] SYP is an integral SV membrane protein that is responsible for the generation of small vesicles.[25] SYP contains a cytoplasmic IDR enriched in aromatic residues (Figures 1B, 2, SI Appendix Figure S2C). We hypothesized

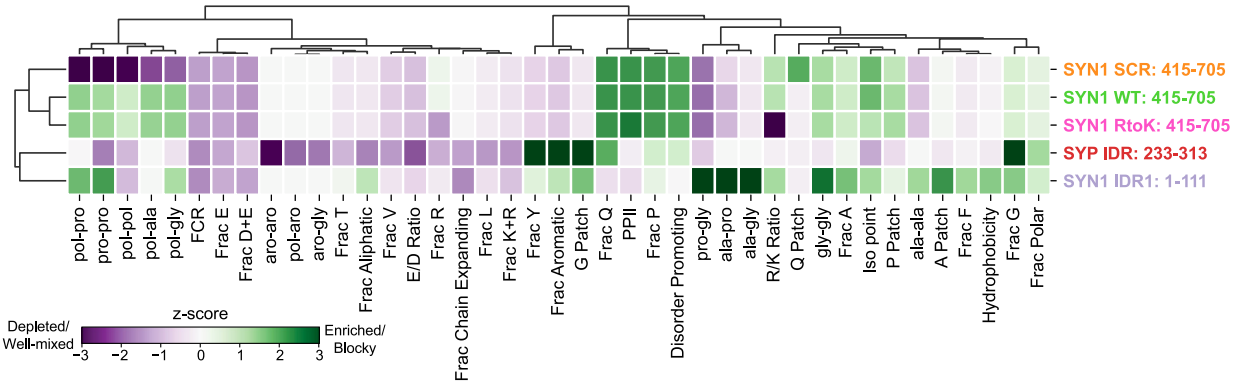

Figure 2. Cluster map of NARDINI+ z-score vectors of SYP IDR, SYN1 IDR1, SYN1 IDR2, and the SYN1 IDR2 variants examined in this study. Only features in which at least one |z-score|≥1 are shown.

that the distinct grammars of the C-terminal IDR of synapsin-1 and the SYP IDR should enable complementary networks of cation-pi-pi interactions.[24] We tested this hypothesis by co-expressing WT synapsin-1 and the synapsin-1 variants with SYP in cells.

Consistent with previous results, we find that co-expression of mCherry-tagged WT synapsin-1 with SYP leads to co-condensation in cells, whereas synapsin-1 remains soluble in the absence of SYP (Figure 3E, SI Appendix Figure S3).[6] In contrast, condensates failed to form when we co-expressed the SCR variant of synapsin-1. Instead, this variant showed a gain-of-function phenotype characterized by co-localization with cytoskeleton elements (Figure 3F–G). This localization pattern was maintained even in the absence of SYP (SI Appendix Figure S3). Together, these results suggest that the non-random and conserved patterning of polar and proline residues mediates the synapsin-1 interaction network.

The substitution of arginine with lysine in the synapsin-1 IDR abrogated co-condensation with SYP in cells (Figure 3E). Therefore, even though lysine and arginine are basic residues, arginine and lysine are not interoperable in the context of the C-terminal IDR of synapsin-1. It appears that the interactions between SYP and synapsin-1 are dominated by complementary cation-pi-pi interactions rather than complementary electrostatic interactions alone.[8] Overall, disrupting the distinct molecular grammars in the synapsin-1 IDR change the interaction network and phase separation of synapsin-1 in cells.

Previous studies showed that the synapsin-1 C-terminal IDR is sufficient for phase separation *in vitro* in the presence of crowders. This result suggests that although homotypic interactions do not drive phase separation in cells, homotypic, depletion-mediated[26] synapsin-1 interactions likely still contribute to the overall in cell phase behavior. Thus, it is important to understand the effects of modulating molecular grammars on synapsin-1 homotypic phase behavior. To accomplish this, we turned to *in vitro* characterizations of phase behaviors, where we cloned, expressed, and purified WT synapsin-1 and the two variants. All proteins have an EGFP fluorescent tag (Figure 3C, SI Appendix Figure S4). In the presence of 3% PEG 8000 we used microscopy to characterize the micron-scale assembles formed by 8 μM of each of the three proteins in 25 mM Tris-HCl (pH 7.4), 0.5 mM TCEP, and 150 mM NaCl. The WT and the two variants showed stark differences in their ability to form condensates. WT synapsin-1 readily formed condensates of 2–3 μm in diameter, whereas the SCR variant formed smaller condensates of up to ~1 μm in diameter. These micron-scale condensates were not observed for the RtoK mutant construct under identical solution conditions (Figure 3D). It is clear that substitution of arginine to lysine weakens depletion-mediated homotypic interactions that abolish the formation of micron-scale assemblies.[17,27–35] Similar results were observed in the presence of 10% Ficoll 400 (SI Appendix Figure S5), suggesting that phase separation in the presence of crowders does not depend on the type of crowder.

Next, we turned to identifying the drivers of synapsin-1 phase separation in the presence of crowders. Using NARDINI+, we find that the sequence grammar of the N-terminal IDR of synapsin-1 shares greater similarity with the SYP IDR when compared to the C-terminal IDR of synapsin-1 (Figure 2). Specifically, the N-terminal IDR is enriched in aromatic residues but to a weaker extent than the SYP IDR. This suggests that interactions between the N- and C-terminal IDRs may be important for synapsin-1 phase separation in the absence of other proteins. To test this hypothesis, we used FINCHES, an algorithm designed to predict IDR-mediated intermolecular interactions.[36] The prediction is that the hydrophobic N-terminus of the N-terminal IDR of synapsin-1 preferentially interacts with the WT C-terminal synapsin-1 IDR (SI Appendix Figure S6A). This interaction is predicted to be similar for the SCR variant, but weakened for the RtoK variant.

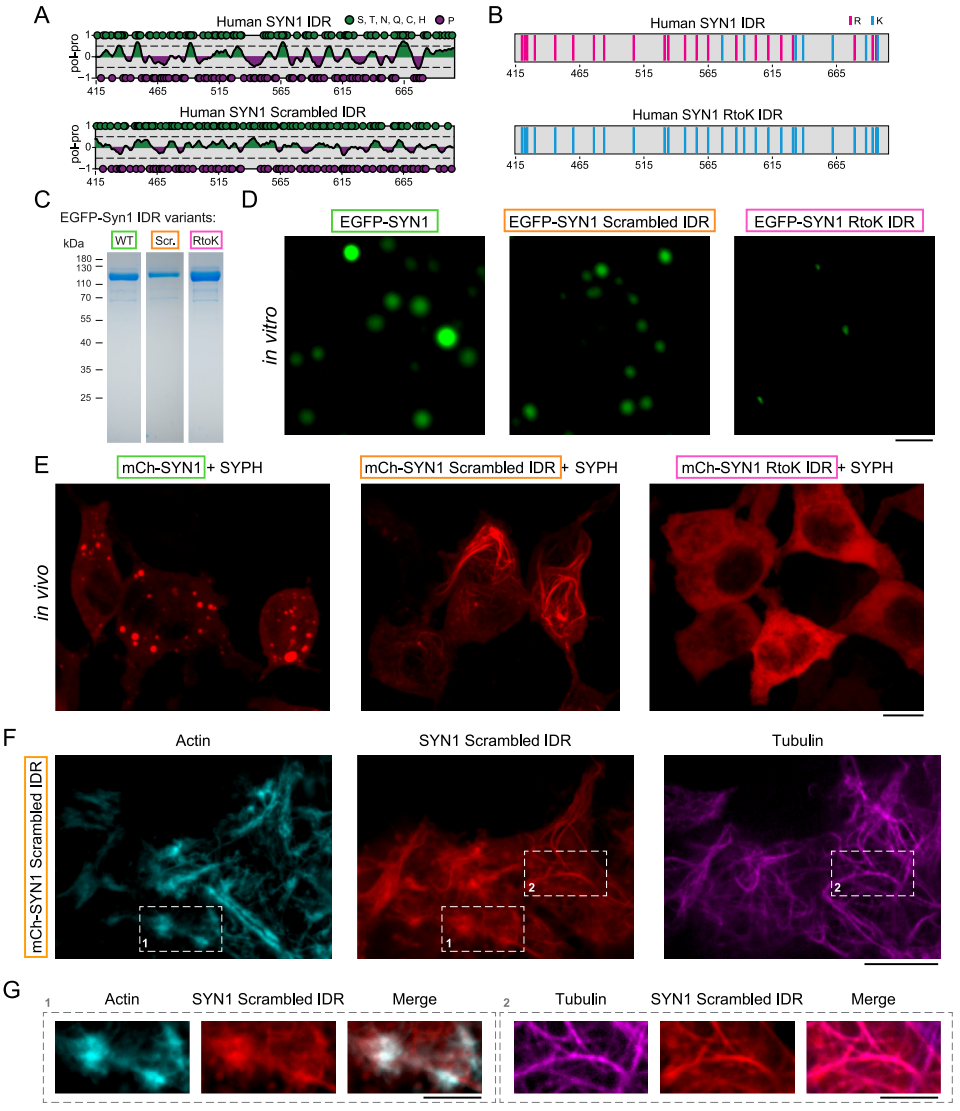

Figure 3. Disruption of the conserved molecular grammars within the C-terminal IDR of synapsin-1 can weaken or abrogate condensate formation *in vitro* and in cells. A. Schematic showing the synapsin-1 scrambled IDR in which polar and proline blocks are evenly distributed to reduce their segregation along the linear sequence. **B.** Schematic of the synapsin-1 IDR showing the substitution of Arg with Lys. **C.** Coomassie gel indicating the final recombinant proteins used for the biophysical assays. **D.** Microscopy images of EGFP-synapsin-1 (8 μM) with WT, SCR, and RtoK IDR reconstituted in 25 mM Tris-HCl (pH 7.4), 0.5 mM TCEP, 150 mM NaCl and 3% PEG 8,000. Scale bar, 5 μm. **E.** Images of HEK cells co-expressing mCherry-tagged synapsin-1 WT (left), scrambled IDR (middle), or RtoK IDR (right) with untagged synaptophysin. Mutants disrupted the formation of normal synapsin condensates. Expression of synapsin-1 designed to have its C-terminal scrambled leads to the formation of filaments that resemble those of cytoskeleton, whereas the RtoK substitutions in this IDR completely abolished condensation. Scale bar: 10 μm. **F.** Image of HEK cells expressing mCherry-tagged synapsin-1 scrambled IDR (middle) co-stained with CellMask™ Green Actin Tracking Stain (for actin, left) and SiR-tubulin (for microtubules, right). Scale bar: 10 μm. **G.** Magnified regions from *F* highlighting the colocalization of synapsin-1 scrambled IDR with actin (left, 1) and microtubules (right, 2). Scale bar: 5 μm.

Given that SCR showed differences in condensation compared to WT and the C-terminal IDR is sufficient for phase separation *in vitro*, phase separation of synapsin-1 in the presence of crowders is not likely to be just the result of interactions between the two IDRs in synapsin-1. Accordingly, we also used FINCHES to identify predicted interactions involving the synapsin-1 C-terminal IDR alone.

The WT synapsin-1C-terminal IDR has a region enriched in proline, glutamine, arginine, and histidine residues that is predicted to be drive interactions between pairs of the same IDR (SI Appendix Figure S6B). Distributing polar and

proline residues uniformly across the sequence, as in the SCR variant, reduces the predicted intra- and inter-IDR interactions involving this region. Thus, although the chemical groups remain unchanged between WT and SCR, the patterning of the chemical groups gives rise to differences in predicted intra- and inter-IDR interactions. Furthermore, consistent with experimental results, the predicted intra- and inter-IDR interactions are generally repulsive for the RtoK variant.

Consistent with the in-cell data, FINCHES predicted that heterotypic interactions between the synapsin-1 IDRs and the SYP IDR are more attractive than inter-IDR interactions of synapsin-1 alone (SI Appendix Figure S6C–D). It is noteworthy that the regions that are predicted to be most attractive in homotypic interactions are the same as those predicted to be most attractive in heterotypic interactions. Lastly, we note that synapsin-1 can form homo- and hetero-dimers with other synapsins.[37] Dimerization has the potential to enhance phase separation by increasing the valency of regions that drive phase separation, such as the synapsin-1 C-terminal IDR.[38]

Synapsin-1 IDR grammars directly affect driving forces for phase separation

To obtain rigorous quantification of driving forces for homotypic phase separation, we mapped comparative phase boundaries for the synapsin-1 variants using a microfluidics-based "PhaseScan" approach[39] (Figure 4A). Phase separation is defined by the presence of threshold concentrations or threshold solubility products depending on whether homotypic versus heterotypic interactions drive the process.[40,41] Measuring phase boundaries requires a scan in concentration space to delineate the one- and two-phase regimes. Synapsin-1 WT, synapsin-1 SCR, and synapsin-1 RtoK each showed distinct phase boundaries (Figure 4**B**). Scrambling the C-terminal IDR of synapsin-1 and/or R-to-K substitutions within the IDR significantly weakened the driving forces for phase separation. This is clear from a rightward shift of the phase boundaries towards higher PEG concentrations, a decrease in the slope, and changes in the shape of the coexistence curves (Figure 4C). The altered shapes of phase boundaries and weakened sensitivity to changes in protein and PEG concentrations

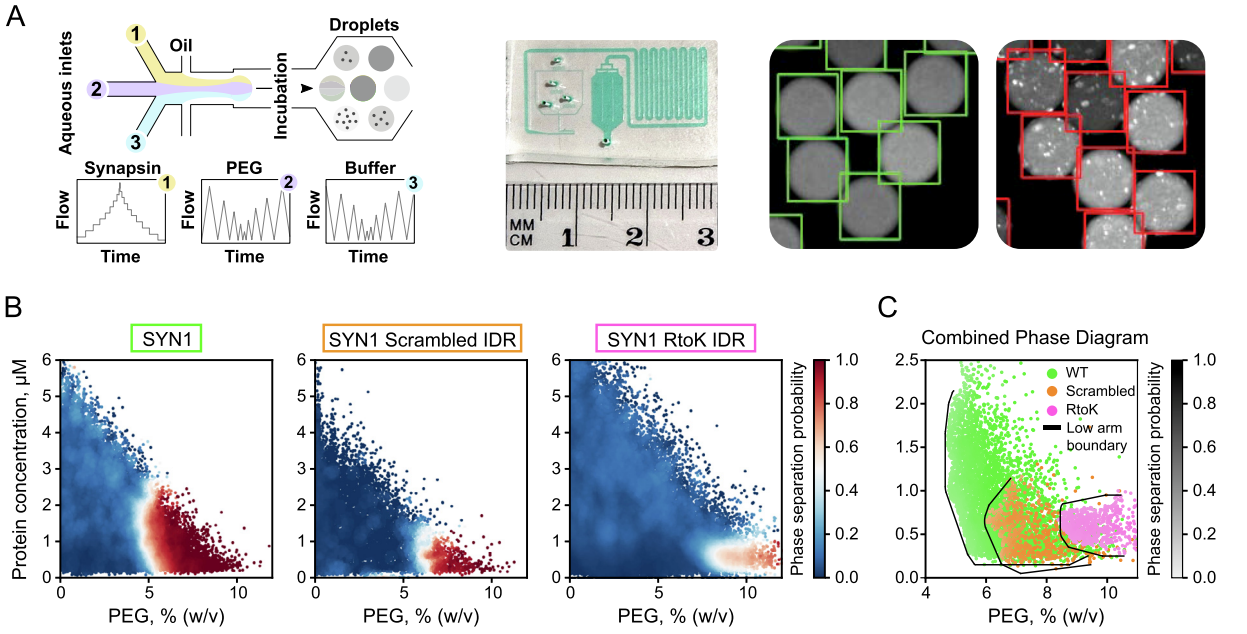

Figure 4. Molecular grammars of synapsin-1 IDR influence synapsin-1 condensation. A. Left: scheme of the microfluidic chip. The insets 1, 2, and 3 are flow rates of synapsin-1, PEG and buffer. Middle: an exemplary photograph of the chip (filled out with a colored solution to highlight the device features). Right: micrographs of individual droplets containing either mixed (green squares) or phase separated (red squares) solution. Classification is performed on each individual droplet as described in Methods. **B.** Low concentration arms of phase boundaries of EGFP-synapsin-1 WT (left, $N = 29{,}187$ points), EGFP-synapsin-1 scrambled IDR (middle, $N = 13{,}203$ data points), or EGFP-synapsin-1 RtoK IDR (right, $N = 64{,}675$ data points). Red and blue data points correspond to individual microdroplets classified as phase separated or homogeneous, respectively. The heatmap quantifies the phase separation probability. **C.** Combined phase boundaries from **A** showing the low concentration arm. The boundaries are drawn using an algorithm, that segregates the measured points that belong to the one-phase versus two-phase regimes.

point to decreased dominance of homotypic interactions[42] engendered by scrambling the sequence and/or arginine to lysine substitutions.

Impact of synapsin-1 IDR grammars on clusters formed in subsaturated solutions

Condensation combines reversible binding, phase separation, and percolation.[14,17,43–45] The formation of cluster phases, as kinetic intermediates, cannot be ruled out as contributors to condensation.[46] Percolation is a networking transition, whereas phase separation is a density transition of the entire solution.[43] One signature of percolation is the formation of heterogeneous distributions of pre-percolation clusters in subsaturated solutions.[15,16,47] Subsaturated solutions refer to concentrations that are below the threshold for phase separation. Note that the origins of clusters in subsaturated solutions are likely to be system-specific depending on the type of physical system (associative polymers, block copolymers, branched polymers, etc.) onto which the proteins of interest can be mapped.[48] Pre-percolation clusters form as the result of encoded hierarchies of so-called sticker versus spacer mediated interactions.[15,16,43] Stickers refer to cohesive domains, motifs, or residues and spacers are interspersed between stickers that modulate the overall solubility of sticker-and-spacer containing sequences.[43] The average sizes of pre-percolation clusters typically increase with increasing concentrations. Furthermore, the distributions of cluster sizes are heavy-tailed implying that the dominant clusters are oligomers, whereas the ultra-low likelihood species are clusters comprising hundreds of molecules.[15,16]

Percolation and phase separation are governed by two different sets of interactions that can be strongly coupled, weakly coupled, or decoupled from one another.[43,49,50] The strengths of reversible associations between stickers determine the percolation threshold and the concentration-dependent size distributions of pre-percolation clusters. These clusters grow continuously with concentration and become system-spanning above the percolation threshold.[43,45] In contrast, phase separation is governed by solubility considerations, which is quantified by the Flory-Huggins χ parameter.[51,52] A requirement for phase separation is that $\chi > 0.5$, and the solubility limit, which defines the saturation concentration or solubility product is set by the magnitude of χ.

Overall, the valence of stickers and the strengths of attractive interactions between stickers set the percolation threshold and the concentration-dependent evolution of the size distributions of pre-percolation clusters. The Flory-Huggins χ parameter, which is governed jointly by the solvation preferences of spacers that are interspersed between stickers and sticker-sticker interactions will determine the driving forces for phase separation.

We deployed microfluidics resistive pulse sensing (MRPS)[53,54] to quantify size distributions of clusters in subsaturated solutions.[15] In MRPS, individual particles in a sample flow through a nanoconstriction across a potential drop in a microfluidic cartridge. The changes to the electrical resistance over the transit time of the particle are used to calculate the particle concentration and diameter, respectively.[54] This method, which is label-free, enables the quantification of sizes ranging from 70 nm to 10 μm.

Substitution of arginine to lysine alters the size distributions of clusters in subsaturated solutions showing a pronounced shift toward smaller species (Figure 5A, B). This points to weakened intermolecular associations that weaken both

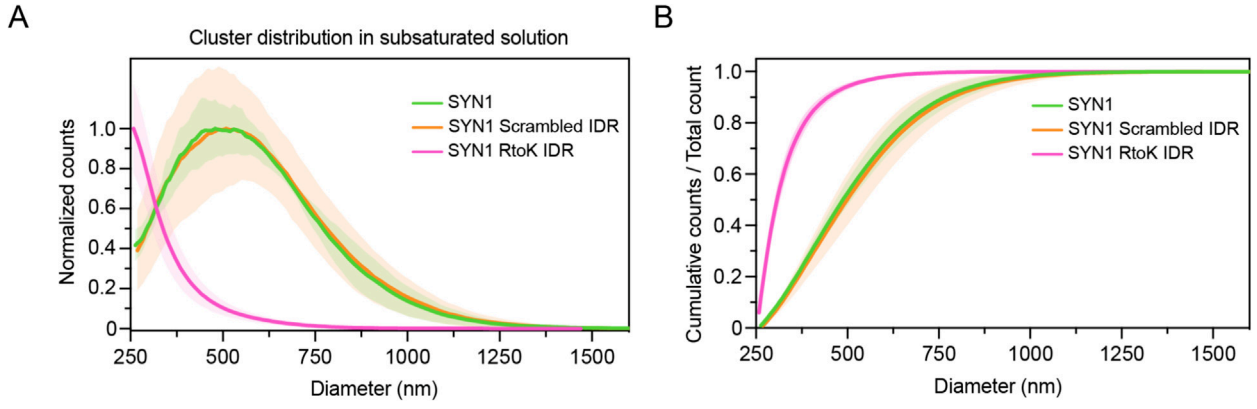

Figure 5. Comparative assessments of cluster size distributions in subsaturated solutions. A. Cluster size distributions in subsaturated solutions for synapsin-1 WT (green), SCR (orange), and RtoK (magenta) variants. Measurements were performed at equivalent conditions (8 μM for each synapsin-1 variant with 3% PEG 8000 in 25 mM Tris-HCl pH 7.4, 150 mM NaCl, 0.5 mM TCEP) using a C-2000 cartridge in an nCS1 instrument. The plot shows the counts that are normalized to the maximum value as a function of the particle diameter. **B.** Cumulative counts for cluster size distributions shown in A. Error bars (shaded) represent standard errors about the mean values.

clustering in subsaturated solutions and the driving forces for phase separation. The latter is manifest as increased threshold concentrations for phase separation, requiring higher concentrations of PEG (Figure 4A, B). In contrast, even though the driving forces for phase separation are weakened when the sequence of the IDR is scrambled in the SCR variant, clustering in subsaturated solutions is equivalent for synapsin-1 WT and synapsin-1 SCR. This implies that the driving forces for forming pre-percolation clusters and phase separation are decoupled by scrambling of the proline and polar blocks. This stands to reason, because in mean-field models, the percolation threshold and hence the extent of clustering are governed purely by the valence and type of stickers that is governed by the composition, which remains unchanged for the SCR variant. However, the solubility limit, which sets the threshold for density transitions,[43] which is known to be affected by the patterning of stickers and spacers of different types,[27,55–58] is altered by scrambling polar and proline residues. This is because the entirety of the sequence, not just the composition, contributes to setting the sequence-specific solubility limit. This is an important finding because it is one of the few instances showing how contributions to clustering in subsaturated solutions and the driving forces for phase separation can be decoupled. It highlights that while intrinsic valence, and hence composition, contributes to clustering and percolation, the overall solubility is governed by patterning, thus emphasizing the contributions of the entirety of the protein sequence.

Interphase pH gradients in synapasin-1 condensates

Biomolecular condensates are defined by two or more coexisting phases. Chemical potentials of all solution components are equalized across the phase boundary, and preferential interactions of solutes or ions such as protons with molecules in the dense or dilute phase can generate passive interphase potentials[59] and pH gradients.[14] We asked if phase separation of synapsin-1 generates a pH gradient. This is because maintenance of a pH gradient is likely to be essential for vesicular ATPase functions and loading of neurotransmitters into SVs.[60,61]

To determine if there is an interphase pH gradient and assess how this might be affected by designed mutations to the IDR of synapsin-1, we employed ratiometric pH-sensitive dyes.[14] These measurements are based on the use of ratiometric Seminaphtharhodafluor (SNARF) dyes, specifically SNARF-1 and SNARF-4. If protons preferentially bind to molecules in the dense phase, then at equilibrium, there will be a passive, interphase proton (pH) gradient making the dense phase more acidic than the coexisting dilute phase. The converse will be true if protons bind preferentially to molecules in the dilute phase.

Using the ratiometric pH-sensitive dye SNARF-1 (Figure 6A–C), we found that synapsin-1 WT, SCR, and RtoK showed equivalent abilities to accumulate protons in dense phases (Figure 6D). Therefore, while molecular grammars in synapsin-1 control driving forces for condensation, the interphase pH gradients remain unchanged, presumably because sequences have an identical net charge.[14]

Discussion

Our studies show that the conserved molecular grammars within the C-terminal IDR of synapsin-1 influence condensation via homotypic interactions *in vitro* and co-condensation with SYP in cells. Computational analysis based on the FINCHES algorithm[36] shows how homotypic and heterotypic interactions are likely to contribute to the observations *in vitro* and in cells. Arginine residues are necessary to drive homotypic and heterotypic interactions that cannot be accounted for purely due to arginine being a basic residue. Instead, arginine is a stronger sticker than lysine due to its pi-like character and stronger cation-pi-pi interactions[24] that can engage with aromatic residues in synapsin-1 and other pre-synaptic proteins.

The segregation of polar and proline residues into distinct blocks is also necessary for homotypic associations and for proper cellular interactions of synapsin-1. Blocks of polar residues may contribute to homotypic interactions,[10,62,63] whereas proline-rich regions can contain motifs that interact with SH3 domain containing pre-synaptic proteins such as intersectin.[1,64] In contrast, the formation of pre-percolated clusters in subsaturated solutions does not depend on segregation of polar and proline residues.

Although the focus of our study has been on the IDR of synapsin-1, our approach can be applied to study how interactions between various pre-synaptic proteins modulate the formation and regulation of SV condensates. Approximately half of the SV resident and soluble SV accessory proteins contain IDRs, and these two sets of pre-synaptic proteins contain distinct and complementary IDR grammars (Figure 1A). We propose that SV clustering is regulated by interactions involving chemical complementarity that is distributed across IDRs of different pre-synaptic proteins. There is support for this hypothesis given that the SV resident proteins SYP, VGLUT1, and VAMP2 and the accessory protein α-synuclein have all been shown to modulate SV clustering.[65–70] Additionally, a recent study showed that resident proteins SYP, SYNGR1, and SYNPR can co-condense SVs with synapsin-1.[71] Our analysis shows that the cytoplasmic C-terminal IDRs of these three proteins cluster

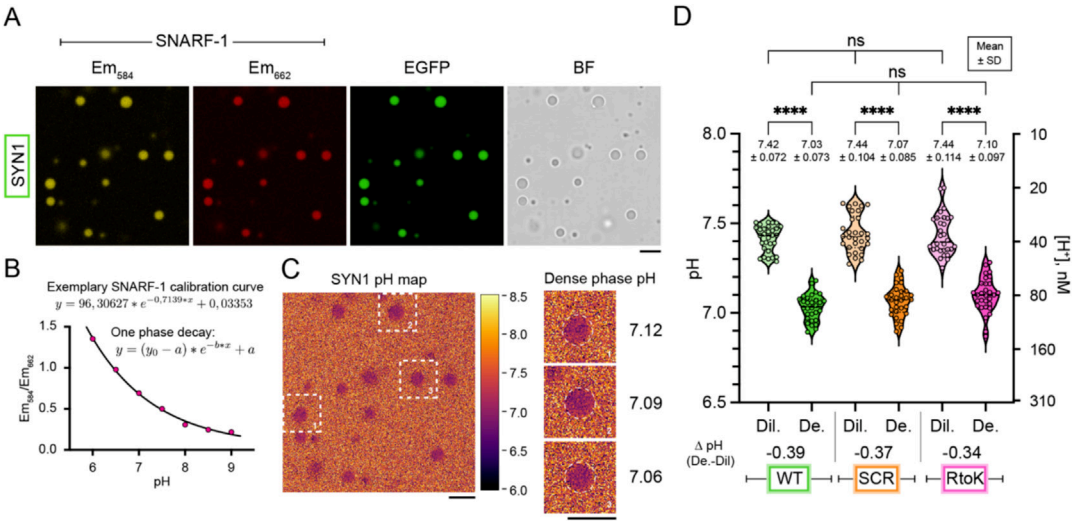

Figure 6. Synapsin-1 condensates sequester protons and lower pH. A. Representative micrographs of EGFP-synapsin-1 condensates (8 μM protein in 3% PEG 8,000) co-incubated with the ratiometric pH-sensitive reporter SNARF-1. SNARF-1 was excited at 561 nm and recorded at 582–586 (yellow) and 660–664 nm (red). Scale bar, 5 μm. **B.** Carboxy SNARF-1 calibration curve for reconstitution buffer (25 mM Tris–HCl, 150 mM NaCl, 0.5 mM TCEP) at different pH (pH 6–9) from a single plane. Data were fit to a one-phase-decay function. **C.** Left: Example micrograph indicating a pH map for EGFP-synapsin-1 WT condensates calculated by applying the z-slice calibration curve. Heatmap represents pH. Right: Magnified regions of selected condensates (dashed line) with indicated average pH values of the dense phase. Scale bar, 5 μm. **D.** pH analysis for the dense and dilute phases of condensates for synapsin-1 WT (green), SCR (orange), and RtoK (magenta) variants. Average pH values are shown in the graph with standard deviation. Violin plots with median and quartiles indicated by the dashed lines. (One-way ANOVA, ****: $p < 0.0001$).

separately from the other SV condensate modulating pre-synaptic proteins due to their enrichment in aromatic residues (Figure 1B). In contrast, VAMP2, which houses an IDR with molecular grammars that are shared with synuclein-1, cannot form condensates with synapsin-1 in cells.[6] However, VAMP2 can be recruited into co-condensates of synuclein-1 and SYP. These results are consistent with chemically complementary features, including cation-π interactions, driving SV condensation, whereas like grammars may play more modulatory roles.

In the context of the pre-synapse, the results presented here and investigations of the synergies of molecular grammars in synaptic boutons[5] are likely to enable new insights into our understanding of the neuronal transmission that is relevant in healthy brains and in diseases characterized by the loss of functional synapses.

Material and Methods

Analysis of IDRs using NARDINI+

Sequence grammars were analyzed using NARDINI+.[14] Briefly, NARDINI+ calculates z-scores of compositional and patterning grammar features previously shown to be important for IDR conformation, interactions, and function.[20] Five additional compositional features were examined that were not described in King et al. These include the number of positive, negative, polar, aliphatic, and aromatic residues, giving a readout on valence compared to the full IDRome. For a given IDR, compositional z-scores are calculated by extracting the compositional feature of the given IDR and using the mean and standard deviations from the full human IDRome (24508 IDRs). The human IDRome contains all IDRs of length ≥30, extracted from the UniProt human proteome (UP000005640) and MobiDB predictions.[72,73] To calculate the patterning z-scores for a given IDR, we deployed the NARDINI algorithm.[12] Here, the linear segregation versus mixing of pairs of residue types in a given IDR sequence is compared to the mean and standard deviations of 10^5 random sequences of the same composition.

Extraction of condensate-specific enriched grammar features

Condensate specific protein lists were extracted from various sources and cross-referenced with the human IDRome to extract condensate-specific IDRs. As described in 14, proteins localized to nucleoli and nuclear speckles were extracted from the Human Protein Atlas (HPA). Proteins localized to P-bodies and stress granules were extracted from 74 and 75, respectively. Synaptic vesicle proteins were extracted from 22 using the list of "SV-resident" proteins leading to 125 IDR sequences.

Proteins buffered by SV proteins were extracted from 23 (here paralogs were included) to yield 47 IDRs. To determine which features were enriched in specific condensates, the human IDRome was split into two sets: (1) the current condensate-specific IDR set and (2) the remaining human IDRome. Then, the distributions for each of the 90 different z-scores were compared using the two-sample Kolmogorov-Smirnov test and a p-value was calculated. The signed $\log_{10}(p\text{-value})$ was calculated for p-values < 0.05. Specifically, $-\log_{10}(p\text{-value})$ was calculated if the condensate-specific mean z-score value was greater than the rest of the IDRome mean z-score value, and $\log_{10}(p\text{-value})$ was calculated if the condensate-specific mean z-score was smaller. Thus, positive values imply the given feature is enriched or blockier in the condensate-specific IDR set.

Extraction of IDR grammar clusters within SV proteins

Feature z-scores were calculated using NARDINI + as described above for IDRs of SV proteins including: SNCA, SNCB, SNCG, SYN1, SYN2, SYN3, SYP, SYNPR, SYNGR1, SV2A, SV2B, SV2C, STX7, VAMP1, VAMP2, VGLUT1, VGLUT2, and VGLUT3. Figure 1B shows a filtered set of enriched features for the four clusters having at least 3 IDRs determined by hierarchical clustering using the Euclidean distance and Ward's linkage method.[76]

Evolutionary analysis of synapsin IDRs

The list of eukaryotic orthologous SYN1 orthologs were extracted from EggNOG.[77] The proteomes of 12 additional species were examined for orthologs if not included in the original EggNOG list. These include *Aptenodytes forsteri* (taxid: 9233), *Doryteuthis pealeii* (taxid: 1051067), *Lampetra fluviatilis* (taxid: 7748), *Leptonychotes weddellii* (taxid: 9713), *Marmota marmota marmota* (taxid: 9994), *Microcebus murinus* (taxid: 30608), *Octopus vulgaris* (taxid: 6645), *Petromyzon marinus* (taxid: 7757), *Physeter macrocephalus* (taxid: 9755), *Urocitellus parryii* (taxid: 9999), Ursus americanus (taxid: 9643), and *Ziphius cavirostris* (taxid: 9760) whose proteomes were extracted from UniProt. BLASTp was used to extract only the most similar ortholog per species as compared to the full SYN1 sequence.[72,78] Then, MUSCLE sequence alignment was utilized to align orthologous sequences.[79] From the alignments, Jalview was used to extract the IDR regions in orthologs corresponding to residues 415–705 of human SYN1.[80] Only orthologous sequences of length $\geq$ 15 and housing no unnatural amino acids were kept. NARDINI+ was then ran on all orthologous sequences where the human IDRome was used as the prior to extract the z-scores of the compositional features. Overall, 152 species were analyzed.

Design of the synapsin-1 scrambled variant

The scramble IDR sequence was created by making 10^5 sequence scrambles where only the positions of residues P, Q, N, S, T, C, H were allowed to be shuffled, whereas all other residue positions were held fixed. Then, we calculated the polar$\equiv$(Q, N, S, T, C, H) versus proline patterning using the pol-pro NARDINI z-score for all 10^5 sequence scrambles. We choose the scramble with the lowest signed z-score. To put this in context, the C-terminal IDR of WT synapsin-1 has a z-score of +1.4, which points to a preference for linear segregation of the polar and proline residues when compared to a random patterning of these residues. In contrast, the C-terminal IDR in the SCR variant has a z-score of -3.5. The negative z-score implies that the proline and polar residues are considerably more well-mixed – by more than three standard deviations – when compared to the random prior, which would have a z-score $\approx$ 0. The ensemble of sequences that fit the design criteria includes sequences with a wide range of z-scores. However, as far as the degree of mixing of polar and proline residues is concerned, the SCR variant features a C-terminal IDR with lowest negative value for the corresponding z-score.

Calculation of mean net residue type profiles

Here, we consider residue types pol$\equiv$(C, H, N, Q, S, T) and pro$\equiv$P. For a given sequence, the fraction of pol residues minus the fraction of pro residues is calculated for each sliding window of length five. Then, the values from all sliding windows that contain a given residue are averaged to yield a residue specific mean net residue type value. These values are plotted in Figures 3A and S1C.

Prediction of IDR interactions using FINCHES

FINCHES is an algorithm that predicts the intermolecular interaction map for a pair of IDRs using the chemical physics encoded in a coarse-grained forcefield.[36] To deploy FINCHES, we utilized the Google Collab notebook (https://colab.research.google.com/drive/1WuzvCnRmOiq4nQFY-fEeETSnrACBuv7kG?usp=sharing). The Mpipi-GG forcefield and a window size of 31 residues were used to extract the interaction maps between SYN1 IDR1, SYN1 IDR2 WT, SYN1 IDR2 SCR, SYN1 IDR2 RtoK, and SYP IDR. Then, the mean of the interaction map was calculated for SYN1 IDR1 or SYN1 IDR2 (and its variants) to determine which regions along the SYN1 IDRs were predicted to be most interaction prone.

Cloning of synapsin 1 IDR variants

Human synapsin-1 coding sequence is based on the NM_006950.3 NCBI reference Sequence. The

complexity of the sequence, such as GC-rich regions, was manually altered to allow efficient gene synthesis while leaving the amino acid sequence unchanged (NP_008881.2). An endogenous *Sac*I restriction site at codons E408-E409 (GAGCTC) was silenced by altering the nucleotide sequence to GAGCTG. To allow for easy subsequent exchange of the synapsin-1 IDR, a *BamH*I was added at codons G389-S390 by changing the nucleotide sequence from GGTTCC to GGATCC. The optimized human synapsin-1 codon sequence and the variant IDR sequences (a.a. 389–705) were created by gene synthesis (Eurofins, HIFI DNA assembly). Subsequently, IDR fragments starting from a.a. 389 were subcloned using the restriction sites *BamH*I and *Sac*I, yielding sequences of full-length Synapsin 1 containing IDR variants. The resulting full-length synapsin-1 sequences (WT, scrambled IDR, RtoK IDR) were either subcloned into a pCMV expression plasmid as a C-terminal fusion protein to mCherry for microscopy[4] by *Kpn2*I and *Sac*I or subcloned into a His14-SUMO_Eu1-EGFP-MCS plasmid for protein purification by *Bgl*II and *Kpn*I.[3] All constructs were verified by Sanger sequencing.

Cell culture and transfection

HEK 293T cells were grown in Dulbecco's Modified Eagle's Medium GlutaMAX supplement (10566016, Gibco) supplemented with 10% fetal bovine serum (12106C, Sigma), 1% MEM Non-essential Amino Acid Solution (M7145, Sigma) and 1% penicillin/streptomycin (15140122, Gibco) at 37 °C and 5% CO_2. For imaging, cells were seeded on 25 mm cover glasses. Cells were transfected with a total of 2 μg of plasmid DNA using Lipofectamine 2000 (11668500, Invitrogen) following the manufacturer's instructions. In brief, the final transfection mixture contained 3 μL of lipofectamine with 2 μg of total plasmid DNA in 200 μL OptiMEM (31985070, Gibco). Transfection mix was incubated for 20 min at room temperature before adding to seeded HEK cells (confluency ~60–70%) and incubated overnight at 37 °C and 5% CO_2. For protein purification experiments, Expi293F™ suspension cultures (A14527, Gibco) were maintained in Expi293™ Expression Medium (A1435102, Gibco) according to the manufacturer's protocol (37 °C, 8% CO_2, 125 rpm). Transfection of suspension cultures (30 mL) was performed with 30 μg of plasmid DNA following the ExpiFectamine™ 293 Transfection Kit guidelines.

Protein expression and purification of synapsin 1 IDR variants

EGFP-tagged synapsin-1 IDR variants were expressed in EXPI cells (HEK derivative) and purified by a two-step purification strategy consisting of NiNTA-affinity and size-exclusion chromatography followed by His-SUMO-tag removal, as described.[3,81] Briefly, His14-SUMO_Eu1-synapsin-1 IDR variants were expressed in Expi293F™cells (Thermo Fisher Scientific) for three days following enhancement. Cells were lysed by three cycles of freezing and thawing in a buffer that contained 25 mM Tris-HCl (pH 7.4), 300 mM NaCl, 0.5 mM TCEP (buffer A) supplemented with EDTA-free Roche Complete protease inhibitors, 15 mM imidazole, 10 μg/mL DNaseI and 1 mM $MgCl_2$. The purification steps were carried out at 4 °C. Lysate clearance was done by centrifugation for 40 min at 30,000*g*. The soluble supernatant was incubated with complete His-Tag Purification resin (Roche) in a polyprep column (Biorad) on a rotating platform for 1 h. Washing steps were done with buffer A with 15 mM imidazole, and elution was performed in buffer A with 400 mM imidazole. Fractions were concentrated using a 30 K MWCO protein concentrator (Millipore) and applied to size exclusion chromatography (Superdex™200 Increase 10/300, GE Healthcare) in a buffer containing 25 mM Tris-HCl (pH 7.4), 150 mM NaCl, 0.5 mM TCEP. Fractions that contained the His14-SUMO_Eu1-Synapsin 1 IDR variant were combined and subjected to tag cleavage with SENP_EuB SUMO protease digest overnight (protease:protein ratio of 1:50) at 4 °C. After incubation, the reaction was supplemented with imidazole and NaCl (final concentrations: 15 mM and 300 mM, respectively). The cleaved His-SUMO-tag and His-tagged SENP protease were removed by passing it three times over preequilibrated (buffer A with 15 mM imidazole) complete His-Tag Purification resin. Proteins in the flow-through were subjected to buffer exchange using a PD-10 column (final buffer: 25 mM Tris-HCl (pH 7.4), 150 mM NaCl, 0.5 mM TCEP) and concentrated with a 30 K MWCO protein concentrator (Millipore). Proteins were snap-frozen in liquid nitrogen and stored at −80 °C until use.

Microscopy and image analysis

For *in vitro* reconstitution of EGFP-Synapsin 1 IDR variants, 8 μM protein was coincubated with polyethylene glycol (PEG 8,000) at a final concentration of 3% in a buffer containing 25 mM Tris-HCl (pH 7.4), 150 mM NaCl and 0.5 mM TCEP. After the addition of PEG, the condensation reaction was transferred to a glass bottom dish (Cellvis D35-20-1.5-N). Imaging was performed on a Nikon spinning disk confocal CSU-X microscope, equipped with a Plan Apo λ 60x Oil objective and a pco.edge camera. The excitation wavelength was 488 nm for EGFP, and image analysis was performed using ImageJ2 (Version: 2.9.0/1.53 t).

For live-cell confocal imaging in HEK cells an Andor DU-888 X-9798 camera and an excitation wavelength at 561 nm were used for mCherry-tagged synapsin-1 IDR variants.

The PhaseScan approach for mapping phase diagrams

The microfluidic devices were fabricated using standard soft-lithography.[39,82] Devices were designed using the AutoCAD (AutoDesk) software and then printed on a photomask (Micro Lithography). To obtain a master with microchannels of approximately 50 μm height, SU-8 3050 (Kayaku Advances Materials) was poured onto a silicon wafer (MicroChem) and spun using a spincoater (Laurell Technologies) for 45 s at 3000 rpm. After soft-baking at 95 °C for 25 min, the wafer with the photomask placed on it was subjected to UV exposure for 60 s. Post-exposure baking at 95 °C for 5 min was then followed by developing with propylene glycol methyl ether acetate (PGMEA, Sigma-Aldrich) and a washing step with isopropanol (IPA, VWR Chemicals). To fabricate the devices, polydimethylsiloxane (PDMS, Sylgard 184) was poured over the master, degassed and then baked at 65 °C for 1.5 h. Subsequently, devices were cut out, and the corresponding holes for the inlets and outlets were punched. A plasma oven (Diener Electronic) was used to treat the devices and enable bonding them to glass slides. The last step was to apply hydrophobic surface modification to the devices using 2% (v/v) trichloro(1H,1H,2H,2H-perfluorooctyl)silane (Sigma-Aldrich) in hydrofluoroether HFE-7500 (Fluorochem).

The PhaseScan microfluidic platform was used to map high-density phase diagrams.[39] The following three aqueous solutions were prepared to be mixed on-chip: 6 μM stock of one of the three EGFP-labelled synapsin-1 variants in 25 mM Tris-HCl (pH 7.4), 150 mM NaCl, 0.5 mM TCEP; solution of the corresponding buffer and a solution of polyethylene glycol (PEG 8000) 10% (w/v) in the same buffer, barcoded with 2 μM Alexa Fluor 647 free dye. Additionally, an oil solution of HFE-7500 (Fluorochem) with 4% surfactant (RAN Biotechnologies) was used for water-in-oil droplet encapsulation. The flow rates of the three aqueous solutions were varied automatically using pressure-controlled pumps (LineUp Flow EZ, Fluigent) according to a pre-programmed flow profile such that each microfluidic droplet contained different concentrations of protein and PEG. The total flow rate of the aqueous solutions was kept constant at 60 μL/h, while the oil flow rate was 150 μL/h, generating droplets of approximately 70 μm in diameter. Droplets were incubated for 3 min before imaging in the same microfluidic chip at two wavelengths (488 nm and 647 nm) at the same time using an epifluorescence microscope (Cairn Research), equipped with a 10x air objective (Nikon CFI Plan Fluor) and a dichroic filter set (Cairn Research). A semi-automated custom-written Python script (Python version 3.9.7) was used to analyze the images, i.e., to detect droplets and classify them as phase separated (1) or mixed (0) by employing a convolution neural network (CNN).[83] To allow calculation of the concentration of the components in each droplet, images of calibration droplets containing only the stock solutions of protein or PEG were recorded. A double-gaussian fit was applied over the fluorescence intensity histograms of the calibration droplets to correlate the intensities back to the stock concentration.[84] Hence, each microfluidic droplet provides information for one data point on the phase diagrams presented as scattered plots. Phase separation probability was further determined for each data point by averaging over its neighboring points within a radius of 5% of the maximum limit of each axis. The boundaries were determined using a fitting that is based on support vector machine-based methods.

Extracting low concentration arms of phase boundaries

First, we generated a two-dimensional histogram of all points that have a phase separation probability of at least 0.55. To eliminate outliers, if there exists at least three data points for the scramble or RtoK sequences and five data points for the WT sequence in a given bin, then the x and y positions of that bin are kept. The boundary is then drawn using these x and y positions and calculating the convex hull with rounded corners.

Measurements of cluster distribution in the subsaturated solutions

Microfluidic Resistive Pulse Sensing (MRPS) measurements were performed on an nCS1 instrument (Spectradyne LLC, Signal Hill, CA, USA). 8 μM of purified synapsin construct was mixed with 3% PEG 8,000 in buffer (25 mM Tris-HCl (pH 7.4), 150 mM NaCl, 0.5 mM TCEP) in an Eppendorf tube to induce phase separation. 5 μL of samples were measured using C-2000 cartridges, with a measurement range of 250–2000 nm. At least three acquisitions (technical triplicates) were collected and combined for analysis, with each acquisition being collected over 10 min. Control experiments were performed with 3% PEG 8,000, where no significant abundance of particles was detected. The particle size distributions from the triplicate experiments were averaged and the resulting curve was smoothed using the LOWESS method in Prism 10 (GraphPad, Boston, MA, USA).

Analysis of pH in synapsin 1 condensates

The ratiometric pH-sensitive dye, 5-(and-6)-Carboxy SNARF™-1 (C1270, Invitrogen), was dissolved to a final concentration of 10 mM in ddH_2O. For calibration, 25 mM Tris-HCl, 150 mM NaCl, and 0.5 mM TCEP buffer were prepared at different pH values (pH 6.0–9.0, steps: 0.5 pH

units). All calibration curves were taken on the same day as the samples with synapsin-1 condensate were analyzed (all in triplicates). In brief, the calibration buffer was mixed with 20 μM final SNARF-1 dye (5 μL final reaction volume) and placed on a glass bottom dish (Cellvis D35-20-1.5-N). Imaging was performed on a Nikon laser scanning confocal AX NSPARC microscope (Ti2, AX camera, Galvano scanner, 2x line averaging, 1024x1024 px resolution, 1.0 μs dwell time) equipped with a Plan Apo λD 60x oil OFN25 DIC N2 objective. Ratiometric imaging of the SNARF-1 dye was performed by excitation at 561 nm and simultaneous readout of the two GaAsP PTMs with different freely tunable emission bands. The first band was set to 582–586 nm (center wavelength: 584 nm) and the second band was set to 660–664 nm (center wavelength: 662 nm). A total of 20 z-stacks were acquired from the cover glass surface into the buffer solution with a step size of 0.20 μm (total measured relative z-height 4.0 μm). Over the entire pH range, the calibration curves were acquired for each z-stack at the same distance from the surface of the coverglass and fitted to a one-phase decay function using GraphPad Prism 10.

For the pH analysis of EGFP-synapsin-1 IDR variants, 8 μM protein was coincubated with 3% PEG 8,000 and 20 μM SNARF-1 dye in a buffer containing 25 mM Tris-HCl (pH 7.5), 150 mM NaCl and 0.5 mM TCEP. Ratiometric z-stacks were recorded from the cover glass surface with the same step size and ratiometric imaging settings as for the calibration curves. Transmission detection was acquired using the 561-nm laser line. Additionally, imaging of EGFP was performed by excitation at 488 nm and emission at 499–551 nm. Of note, while synapsin-1 WT and scrambled IDR condensates formed readily within minutes, synapsin-1 RtoK IDR variant condensate formation was forced by extending the incubation time on the cover glass to one hour.

For image analysis, each pixel of the 584-nm emission image was divided by the corresponding pixel of the 662-nm emission image for each individual z-stack. The resulting ratio z-stack series was converted to a pH stack by applying the corresponding z-slice calibration curve to each matching ratio z-slice. All measurements were performed in three independent reconstitutions with 10 condensates selected from each single reconstitution. A dense phase ROI was outlined with the segmented line tool in ImageJ, and a corresponding circular dilute phase ROI (diameter: 4.3 μm) was placed 2 μm away from the dense phase. ROIs were selected on a single z-plane. Mean pH values of both dense and dilute phases were plotted as violin plots. One-Way ANOVA tests (multiple comparisons, Tukey, alpha = 0.05) were performed for statistical analysis in GraphPad Prism 10 (GraphPad, Boston, MA, USA).

Author contributions

CH performed reconstitution experiments. **KMR** did the computational analyses. **CH, IAE, HA** performed microfluidic experiments and analyzed the data; **CH** and **MKS** performed MRPS measurements. **CH, MRK, AP** performed pH measurements. **CH** and **JVT** performed cell experiments. **JRM** and **TPJK** contributed to experimental designs. **RVP** and **DM** designed the study and wrote the paper.

CRediT authorship contribution statement

Christian Hoffmann: Writing – review & editing, Writing – original draft, Visualization, Validation, Methodology, Investigation, Formal analysis, Data curation, Conceptualization. **Kiersten M. Ruff:** Writing – review & editing, Writing – original draft, Visualization, Validation, Methodology, Investigation, Formal analysis, Data curation, Conceptualization. **Irina A. Edu:** Writing – review & editing, Visualization, Methodology, Investigation, Formal analysis. **Min Kyung Shinn:** Writing – review & editing, Methodology, Investigation, Formal analysis. **Johannes V. Tromm:** Writing – review & editing, Methodology, Investigation, Formal analysis. **Matthew R. King:** Writing – review & editing, Methodology, Investigation, Data curation. **Avnika Pant:** Writing – review & editing, Methodology, Investigation, Data curation. **Hannes Ausserwöger:** Writing – review & editing, Methodology, Investigation, Data curation. **Jennifer R. Morgan:** Writing – review & editing, Investigation. **Tuomas P.J. Knowles:** Writing – review & editing, Supervision, Resources, Methodology, Investigation, Funding acquisition. **Rohit V. Pappu:** Writing – review & editing, Writing – original draft, Visualization, Validation, Supervision, Software, Resources, Project administration, Methodology, Investigation, Funding acquisition, Data curation, Conceptualization. **Dragomir Milovanovic:** Writing – review & editing, Writing – original draft, Visualization, Validation, Supervision, Resources, Project administration, Methodology, Investigation, Funding acquisition, Data curation, Conceptualization.

DATA AVAILABILITY

Data will be made available on request.

DECLARATION OF COMPETING INTEREST

The authors declare the following financial interests/personal relationships which may be considered as potential competing interests: “RVP is a member of the scientific advisory board and shareholder in Dewpoint Therapeutics Inc. TPJK

is a co-founder of Fluid Analytics, Wren Therapeutics, Xampla, and Transition Bio. All other authors have no competing interests.".

Acknowledgments

We thank the AMBIO Facility at Charité for microscopy. Supported by DZNE, grants from the DFG (MI 2104 and SFB1286/B10 to DM); ERC Grants (101078172 to DM, DiProPhys 101001615 to TPJK); the US National Institutes of Health (NIA 2RF1 NS078165-12 to JRM, NINDS R01NS121114 to RVP, F32GM146418-01A1 to MRK, and K99GM152778 to MKS); the Air Force Office of Scientific Research AFOSR (FA9550-20-1-0241 to RVP); and the US-National Science Foundation (MCB-2227268 to RVP). CH is supported by the Innovative Minds Program of the German Dementia Association.

Appendix A. Supplementary material

Supplementary material to this article can be found online at https://doi.org/10.1016/j.jmb.2025.168987.

Received 7 October 2024;
Accepted 6 February 2025;
Available online 11 February 2025

Keywords:
phase separation;
synapse;
synapsin 1;
microfluidics;
interphase pH gradient

† These authors contributed equally.

References

1. Milovanovic, D., Wu, Y., Bian, X., Camilli, P.D., (2018). A liquid phase of synapsin and lipid vesicles. *Science* **361**, 604–607. https://doi.org/10.1126/science.aat5671.
2. Pechstein, A., Tomilin, N., Fredrich, K., Vorontsova, O., Sopova, E., Evergren, E., Haucke, V., Brodin, L., Shupliakov, O., (2020). Vesicle clustering in a living synapse depends on a synapsin region that mediates phase separation. *Cell Rep.* **30**, 2594–2602.e3. https://doi.org/10.1016/j.celrep.2020.01.092.
3. Hoffmann, C., Rentsch, J., Tsunoyama, T.A., Chhabra, A., Perez, G.A., Chowdhury, R., Trnka, F., Korobeinikov, A.A., Shaib, A.H., Ganzella, M., Giannone, G., Rizzoli, S.O., Kusumi, A., Ewers, H., Milovanovic, D., (2023). Synapsin condensation controls synaptic vesicle sequestering and dynamics. *Nature Commun.* **14**, 6730. https://doi.org/10.1038/s41467-023-42372-6.
4. Hoffmann, C., Sansevrino, R., Morabito, G., Logan, C., Vabulas, R.M., Ulusoy, A., Ganzella, M., Milovanovic, D., (2021). Synapsin condensates recruit alpha-synuclein. *J. Mol. Biol.*166961. https://doi.org/10.1016/j.jmb.2021.166961.
5. Sansevrino, R., Hoffmann, C., Milovanovic, D., (2023). Condensate biology of synaptic vesicle clusters. *Trends Neurosci.*. https://doi.org/10.1016/j.tins.2023.01.001.
6. Park, D., Wu, Y., Lee, S.-E., Kim, G., Jeong, S., Milovanovic, D., Camilli, P.D., Chang, S., (2021). Cooperative function of synaptophysin and synapsin in the generation of synaptic vesicle-like clusters in non-neuronal cells. *Nature Commun.* **12**, 263. https://doi.org/10.1038/s41467-020-20462-z.
7. Südhof, T.C., Lottspeich, F., Greengard, P., Mehl, E., Jahn, R., (1987). A synaptic vesicle protein with a novel cytoplasmic domain and four transmembrane regions. *Science (New York, N.Y.)* **238**, 1142–1144.
8. Kim, G., Lee, S.-E., Jeong, S., Lee, J., Park, D., Chang, S., (2021). Multivalent electrostatic pi–cation interaction between synaptophysin and synapsin is responsible for the coacervation. *Mol. Brain* **14**, 137. https://doi.org/10.1186/s13041-021-00846-y.
9. Gerth, F., Jäpel, M., Pechstein, A., Kochlamazashvili, G., Lehmann, M., Puchkov, D., Onofri, F., Benfenati, F., Nikonenko, A.G., Fredrich, K., Shupliakov, O., Maritzen, T., Freund, C., Haucke, V., (2017). Intersectin associates with synapsin and regulates its nanoscale localization and function. *PNAS* **114**, 12057–12062. https://doi.org/10.1073/pnas.1715341114.
10. Patil, A., Strom, A.R., Paulo, J.A., Collings, C.K., Ruff, K.M., Shinn, M.K., Sankar, A., Cervantes, K.S., Wauer, T., St, J.D., Laurent, G., Xu, L.A., Becker, S.P., Gygi, R.V., Pappu, C.P., Brangwynne, C.K., (2023). A disordered region controls cBAF activity via condensation and partner recruitment. *Cell 186*, 4936–4955.e26. https://doi.org/10.1016/j.cell.2023.08.032.
11. Shinn, M.K., Cohan, M.C., Bullock, J.L., Ruff, K.M., Levin, P.A., Pappu, R.V., (2022). Connecting sequence features within the disordered C-terminal linker of Bacillus subtilis FtsZ to functions and bacterial cell division. *PNAS* **119**, e2211178119. https://doi.org/10.1073/pnas.2211178119.
12. Cohan, M.C., Shinn, M.K., Lalmansingh, J.M., Pappu, R.V., (2022). Uncovering non-random binary patterns within sequences of intrinsically disordered proteins. *J. Mol. Biol.* **434**, 167373. https://doi.org/10.1016/j.jmb.2021.167373.
13. King, M.R., Ruff, K.M., Pappu, R.V., (2024). Emergent microenvironments of nucleoli. *Nucleus* **15**, 2319957. https://doi.org/10.1080/19491034.2024.2319957.
14. King, M.R., Ruff, K.M., Lin, A.Z., Pant, A., Farag, M., Lalmansingh, J.M., Wu, T., Fossat, M.J., Ouyang, W., Lew, M.D., Lundberg, E., Vahey, M.D., Pappu, R.V., (2024). Macromolecular condensation organizes nucleolar sub-phases to set up a pH gradient. *Cell* **187**, 1889–1906.e24. https://doi.org/10.1016/j.cell.2024.02.029.
15. Kar, M., Dar, F., Welsh, T.J., Vogel, L.T., Kühnemuth, R., Majumdar, A., Krainer, G., Franzmann, T.M., Alberti, S., Seidel, C.A.M., Knowles, T.P.J., Hyman, A.A., Pappu, R. V., (2022). Phase-separating RNA-binding proteins form heterogeneous distributions of clusters in subsaturated solutions. *PNAS* **119**, e2202222119. https://doi.org/10.1073/pnas.2202222119.
16. Kar, M., Vogel, L.T., Chauhan, G., Felekyan, S., Ausserwöger, H., Welsh, T.J., Dar, F., Kamath, A.R., Knowles, T.P.J., Hyman, A.A., Seidel, C.A.M., Pappu, R.

V., (2024). Solutes unmask differences in clustering versus phase separation of FET proteins. *Nature Commun.* **15**, 4408. https://doi.org/10.1038/s41467-024-48775-3.
17. Wang, J., Choi, J.-M., Holehouse, A.S., Lee, H.O., Zhang, X., Jahnel, M., Maharana, S., Lemaitre, R., Pozniakovsky, A., Drechsel, D., Poser, I., Pappu, R.V., Alberti, S., Hyman, A.A., (2018). A molecular grammar governing the driving forces for phase separation of prion-like RNA binding proteins. *Cell* **174**, 688–699.e16. https://doi.org/10.1016/j.cell.2018.06.006.
18. Ruff, K.M., Choi, Y.H., Cox, D., Ormsby, A.R., Myung, Y., Ascher, D.B., Radford, S.E., Pappu, R.V., Hatters, D.M., (2022). Sequence grammar underlying the unfolding and phase separation of globular proteins. *Mol. Cell* **82**, 3193–3208.e8. https://doi.org/10.1016/j.molcel.2022.06.024.
19. Mensah, M.A., Niskanen, H., Magalhaes, A.P., Basu, S., Kircher, M., Sczakiel, H.L., Reiter, A.M.V., Elsner, J., Meinecke, P., Biskup, S., Chung, B.H.Y., Dombrowsky, G., Eckmann-Scholz, C., Hitz, M.P., Hoischen, A., Holterhus, P.-M., Hülsemann, W., Kahrizi, K., Kalscheuer, V.M., Kan, A., Krumbiegel, M., Kurth, I., Leubner, J., Longardt, A.C., Moritz, J.D., Najmabadi, H., Skipalova, K., Blok, L.S., Tzschach, A., Wiedersberg, E., Zenker, M., Garcia-Cabau, C., Buschow, R., Salvatella, X., Kraushar, M.L., Mundlos, S., Caliebe, A., Spielmann, M., Horn, D., Hnisz, D., (2023). Aberrant phase separation and nucleolar dysfunction in rare genetic diseases. *Nature* **614**, 564–571. https://doi.org/10.1038/s41586-022-05682-1.
20. Zarin, T., Strome, B., Peng, G., Pritišanac, I., Forman-Kay, J.D., Moses, A.M., (2021). Identifying molecular features that are associated with biological function of intrinsically disordered protein regions. *Elife* **10**, e60220. https://doi.org/10.7554/elife.60220.
21. Ravindran, R., Bacellar, I.O.L., Castellanos-Girouard, X., Wahba, H.M., Zhang, Z., Omichinski, J.G., Kisley, L., Michnick, S.W., (2023). Peroxisome biogenesis initiated by protein phase separation. *Nature* **617**, 608–615. https://doi.org/10.1038/s41586-023-06044-1.
22. Taoufiq, Z., Ninov, M., Villar-Briones, A., Wang, H.-Y., Sasaki, T., Roy, M.C., Beauchain, F., Mori, Y., Yoshida, T., Takamori, S., Jahn, R., Takahashi, T., (2020). Hidden proteome of synaptic vesicles in the mammalian brain. *PNAS* **117**, 33586–33596. https://doi.org/10.1073/pnas.2011870117.
23. Denker, A., Kröhnert, K., Bückers, J., Neher, E., Rizzoli, S. O., (2011). The reserve pool of synaptic vesicles acts as a buffer for proteins involved in synaptic vesicle recycling. *PNAS* **108**, 17183–17188. https://doi.org/10.1073/pnas.1112690108.
24. Vernon, R.M., Chong, P.A., Tsang, B., Kim, T.H., Bah, A., Farber, P., Lin, H., Forman-Kay, J.D., (2018). Pi-Pi contacts are an overlooked protein feature relevant to phase separation. *Elife* **7**, e31486. https://doi.org/10.7554/elife.31486.
25. Cameron, P.L., Südhof, T.C., Jahn, R., Camilli, P.D., (1991). Colocalization of synaptophysin with transferrin receptors: implications for synaptic vesicle biogenesis. *J. Cell Biol.* **115**, 151–164. https://doi.org/10.1083/jcb.115.1.151.
26. Chauhan, G., Bremer, A., Dar, F., Mittag, T., Pappu, R.V., (2024). Crowder titrations enable the quantification of driving forces for macromolecular phase separation. *Biophys. J.* **123**, 1376–1392. https://doi.org/10.1016/j.bpj.2023.09.006.
27. Nott, T.J., Petsalaki, E., Farber, P., Jervis, D., Fussner, E., Plochowietz, A., Craggs, T.D., Bazett-Jones, D.P., Pawson, T., Forman-Kay, J.D., Baldwin, A.J., (2015). Phase transition of a disordered nuage protein generates environmentally responsive membraneless organelles. *Mol. Cell* **57**, 936–947. https://doi.org/10.1016/j.molcel.2015.01.013.
28. Greig, J.A., Nguyen, T.A., Lee, M., Holehouse, A.S., Posey, A.E., Pappu, R.V., Jedd, G., (2020). Arginine-enriched mixed-charge domains provide cohesion for nuclear speckle condensation. *Mol. Cell* **77**, 1237–1250.e4. https://doi.org/10.1016/j.molcel.2020.01.025.
29. Brady, J.P., Farber, P.J., Sekhar, A., Lin, Y.-H., Huang, R., Bah, A., Nott, T.J., Chan, H.S., Baldwin, A.J., Forman-Kay, J.D., Kay, L.E., (2017). Structural and hydrodynamic properties of an intrinsically disordered region of a germ cell-specific protein on phase separation. *PNAS* **114**, E8194–E8203. https://doi.org/10.1073/pnas.1706197114.
30. Fisher, R.S., Elbaum-Garfinkle, S., (2020). Tunable multiphase dynamics of arginine and lysine liquid condensates. *Nature Commun.* **11**, 4628. https://doi.org/10.1038/s41467-020-18224-y.
31. Hong, Y., Najafi, S., Casey, T., Shea, J.-E., Han, S.-I., Hwang, D.S., (2022). Hydrophobicity of arginine leads to reentrant liquid-liquid phase separation behaviors of arginine-rich proteins. *Nature Commun.* **13**, 7326. https://doi.org/10.1038/s41467-022-35001-1.
32. Fossat, M.J., Zeng, X., Pappu, R.V., (2021). Uncovering differences in hydration free energies and structures for model compound mimics of charged side chains of amino acids. *J. Phys. Chem. B* **125**, 4148–4161. https://doi.org/10.1021/acs.jpcb.1c01073.
33. Zeng, X., Ruff, K.M., Pappu, R.V., (2022). Competing interactions give rise to two-state behavior and switch-like transitions in charge-rich intrinsically disordered proteins. *PNAS* **119**, e2200559119. https://doi.org/10.1073/pnas.2200559119.
34. Bremer, A., Farag, M., Borcherds, W.M., Peran, I., Martin, E.W., Pappu, R.V., Mittag, T., (2022). Deciphering how naturally occurring sequence features impact the phase behaviours of disordered prion-like domains. *Nature Chem.* **14**, 196–207. https://doi.org/10.1038/s41557-021-00840-w.
35. Oh, S.-H., Lee, J., Lee, M., Kim, S., Lee, W.B., Lee, D.W., Choi, S.-H., (2023). Simple coacervation of guanidinium-containing polymers induced by monovalent salt. *Macromolecules* **56**, 3989–3999. https://doi.org/10.1021/acs.macromol.2c02346.
36. Ginell, G.M., Ryan, J., Emenecker, J.M., Lotthammer, E.T., Usher, A.S Holehouse, (2024). Direct prediction of intermolecular interactions driven by disordered regions. *BioRxiv*2024.06.03.597104. https://doi.org/10.1101/2024.06.03.597104.
37. Hosaka, M., Südhof, T.C., (1999). Homo- and heterodimerization of synapsins. *J. Biol. Chem.* **274**, 16747–16753.
38. Yang, P., Mathieu, C., Kolaitis, R.-M., Zhang, P., Messing, J., Yurtsever, U., Yang, Z., Wu, J., Li, Y., Pan, Q., Yu, J., Martin, E.W., Mittag, T., Kim, H.J., Taylor, J.P., (2020). G3BP1 is a tunable switch that triggers phase separation to assemble stress granules. *Cell* **181**, 325–345.e28. https://doi.org/10.1016/j.cell.2020.03.046.
39. Arter, W.E., Qi, R., Erkamp, N.A., Krainer, G., Didi, K., Welsh, T.J., Acker, J., Nixon-Abell, J., Qamar, S., Guillén-

Boixet, J., Franzmann, T.M., Kuster, D., Hyman, A.A., Borodavka, A., George-Hyslop, P.S., Alberti, S., Knowles, T.P.J., (2022). Biomolecular condensate phase diagrams with a combinatorial microdroplet platform. *Nature Commun.* **13**, 7845. https://doi.org/10.1038/s41467-022-35265-7.

40. Chattaraj, A., Blinov, M.L., Loew, L.M., (2021). The solubility product extends the buffering concept to heterotypic biomolecular condensates. *Elife* **10**, e67176. https://doi.org/10.7554/elife.67176.
41. Farag, M., Borcherds, W.M., Bremer, A., Mittag, T., Pappu, R.V., (2023). Phase separation of protein mixtures is driven by the interplay of homotypic and heterotypic interactions. *Nature Commun.* **14**, 5527. https://doi.org/10.1038/s41467-023-41274-x.
42. Qian, D., Ausserwoger, H., Sneideris, T., Farag, M., Pappu, R.V., Knowles, T.P.J., (2024). Dominance analysis to assess solute contributions to multicomponent phase equilibria. *PNAS* **121**, e2407453121. https://doi.org/10.1073/pnas.2407453121.
43. Pappu, R.V., Cohen, S.R., Dar, F., Farag, M., Kar, M., (2023). Phase transitions of associative biomacromolecules. *Chem. Rev.* **123**, 8945–8987. https://doi.org/10.1021/acs.chemrev.2c00814.
44. Semenov, A.N., Rubinstein, M., (1998). Thermoreversible gelation in solutions of associative polymers. 1. Statics. *Macromolecules* **31**, 1373–1385. https://doi.org/10.1021/ma970616h.
45. Choi, J.-M., Hyman, A.A., Pappu, R.V., (2020). Generalized models for bond percolation transitions of associative polymers. *Phys. Rev. E* **102**, 042403. https://doi.org/10.1103/physreve.102.042403.
46. Vekilov, P.G., (2012). Phase diagrams and kinetics of phase transitions in protein solutions. *J. Phys. Condens. Matter* **24**, 193101. https://doi.org/10.1088/0953-8984/24/19/193101.
47. Tanaka, F., (2006). *Mol. Gels*, 17–77. https://doi.org/10.1007/1-4020-3689-2_2.
48. Oranges, M., Jash, C., Golani, G., Seal, M., Cohen, S.R., Rosenhek-Goldian, I., Bogdanov, A., Safran, S., Goldfarb, D., (2024). Core-shell model of the clusters of CPEB4 isoforms preceding liquid-liquid phase separation. *Biophys. J.* **123**, 2604–2622. https://doi.org/10.1016/j.bpj.2024.06.027.
49. Rubinstein, M., Semenov, A.N., (1998). Thermoreversible gelation in solutions of associating polymers. 2. Linear dynamics. *Macromolecules* **31**, 1386–1397. https://doi.org/10.1021/ma970617+.
50. Harmon, T.S., Holehouse, A.S., Rosen, M.K., Pappu, R.V., (2017). Intrinsically disordered linkers determine the interplay between phase separation and gelation in multivalent proteins. *Elife* **6**, e30294. https://doi.org/10.7554/elife.30294.
51. Flory, P.J., (1942). Thermodynamics of high polymer solutions. *J. Chem. Phys.* **10**, 51–61. https://doi.org/10.1063/1.1723621.
52. Huggins, M.L., (1941). Solutions of long chain compounds. *J. Chem. Phys.* **9**, 440. https://doi.org/10.1063/1.1750930.
53. Song, Y., Zhang, J., Li, D., (2017). Microfluidic and nanofluidic resistive pulse sensing: a review. *Micromachines* **8**, 204. https://doi.org/10.3390/mi8070204.
54. DeBlois, R.W., Bean, C.P., (1970). Counting and sizing of submicron particles by the resistive pulse technique. *Rev. Sci. Instrum.* **41**, 909–916. https://doi.org/10.1063/1.1684724.
55. Pak, C.W., Kosno, M., Holehouse, A.S., Padrick, S.B., Mittal, A., Ali, R., Yunus, A.A., Liu, D.R., Pappu, R.V., Rosen, M.K., (2016). Sequence determinants of intracellular phase separation by complex coacervation of a disordered protein. *Mol. Cell* **63**, 72–85. https://doi.org/10.1016/j.molcel.2016.05.042.
56. Lin, Y.-H., Chan, H.S., (2017). Phase separation and single-chain compactness of charged disordered proteins are strongly correlated. *Biophys. J.* **112**, 2043–2046. https://doi.org/10.1016/j.bpj.2017.04.021.
57. Dignon, G.L., Best, R.B., Mittal, J., (2020). Biomolecular phase separation: from molecular driving forces to macroscopic properties. *Annu. Rev. Phys. Chem.* **71**, 53–75. https://doi.org/10.1146/annurev-physchem-071819-113553.
58. Martin, E.W., Holehouse, A.S., Peran, I., Farag, M., Incicco, J.J., Bremer, A., Grace, C.R., Soranno, A., Pappu, R.V., Mittag, T., (2020). Valence and patterning of aromatic residues determine the phase behavior of prion-like domains. *Science* **367**, 694–699. https://doi.org/10.1126/science.aaw8653.
59. Hoffmann, C., Murastov, G., Tromm, J.V., Moog, J.-B., Aslam, M.A., Matkovic, A., Milovanovic, D., (2023). Electric potential at the interface of membraneless organelles gauged by graphene. *Nano Lett.*. https://doi.org/10.1021/acs.nanolett.3c02915.
60. Farsi, Z., Preobraschenski, J., van den Bogaart, G., Riedel, D., Jahn, R., Woehler, A., (2016). Single-vesicle imaging reveals different transport mechanisms between glutamatergic and GABAergic vesicles. *Science* **351**, 981–984. https://doi.org/10.1126/science.aad8142.
61. Kosmidis, E., Shuttle, C.G., Preobraschenski, J., Ganzella, M., Johnson, P.J., Veshaguri, S., Holmkvist, J., Møller, M. P., Marantos, O., Marcoline, F., Grabe, M., Pedersen, J.L., Jahn, R., Stamou, D., (2022). Regulation of the mammalian-brain V-ATPase through ultraslow mode-switching. *Nature* **611**, 827–834. https://doi.org/10.1038/s41586-022-05472-9.
62. Crick, S.L., Ruff, K.M., Garai, K., Frieden, C., Pappu, R.V., (2013). Unmasking the roles of N- and C-terminal flanking sequences from exon 1 of huntingtin as modulators of polyglutamine aggregation. *PNAS* **110**, 20075–20080. https://doi.org/10.1073/pnas.1320626110.
63. Kar, M., Posey, A.E., Dar, F., Hyman, A.A., Pappu, R.V., (2021). Glycine-rich peptides from FUS have an intrinsic ability to self-assemble into fibers and networked fibrils. *Biochemistry* **60**, 3213–3222. https://doi.org/10.1021/acs.biochem.1c00501.
64. Li, P., Banjade, S., Cheng, H.-C., Kim, S., Chen, B., Guo, L., Llaguno, M., Hollingsworth, J.V., King, D.S., Banani, S. F., Russo, P.S., Jiang, Q.-X., Nixon, B.T., Rosen, M.K., (2012). Phase transitions in the assembly of multivalent signalling proteins. *Nature* **483**, 336–340. https://doi.org/10.1038/nature10879.
65. Kokotos, A.C., Harper, C.B., Marland, J.R.K., Smillie, K.J., Cousin, M.A., Gordon, S.L., (2019). Synaptophysin sustains presynaptic performance by preserving vesicular synaptobrevin-II levels. *J. Neurochem.* **151**, 28–37. https://doi.org/10.1111/jnc.14797.
66. Gordon, S.L., Leube, R.E., Cousin, M.A., (2011). Synaptophysin is required for synaptobrevin retrieval during synaptic vesicle endocytosis. *J. Neurosci.* **31**, 14032–14036. https://doi.org/10.1523/jneurosci.3162-11.2011.

67. Atias, M., Tevet, Y., Sun, J., Stavsky, A., Tal, S., Kahn, J., Roy, S., Gitler, D., (2019). Synapsins regulate α-synuclein functions. *PNAS* **116**, 11116–11118. https://doi.org/10.1073/pnas.1903054116.
68. Sun, J., Wang, L., Bao, H., Premi, S., Das, U., Chapman, E.R., Roy, S., (2019). Functional cooperation of α-synuclein and VAMP2 in synaptic vesicle recycling. *PNAS* **116**, 11113–11115. https://doi.org/10.1073/pnas.1903049116.
69. Zhang, X.M., François, U., Silm, K., Angelo, M.F., Fernandez-Busch, M.V., Maged, M., Martin, C., Bernard, V., Cordelières, F.P., Deshors, M., Pons, S., Maskos, U., Bemelmans, A.P., Wojcik, S.M., Mestikawy, S.E., Humeau, Y., Herzog, E., (2019). A proline-rich motif on VGLUT1 reduces synaptic vesicle super-pool and spontaneous release frequency. *Elife* **8**, e50401. https://doi.org/10.7554/elife.50401.
70. Jackson, J., Hoffmann, C., Scifo, E., Wang, H., Wischhof, L., Piazzesi, A., Mondal, M., Shields, H., Zhou, X., Mondin, M., Ryan, E.B., Döring, H., Prehn, J.H.M., Rottner, K., Giannone, G., Nicotera, P., Ehninger, D., Milovanovic, D., Bano, D., (2024). Actin-nucleation promoting factor N-WASP influences alpha-synuclein condensates and pathology. *Cell Death Dis.* **15**, 304. https://doi.org/10.1038/s41419-024-06686-7.
71. Park, D., Fujise, K., Wu, Y., Luján, R., Olmo-Cabrera, S.D., Wesseling, J.F., Camilli, P.D., (2024). Overlapping role of synaptophysin and synaptogyrin family proteins in determining the small size of synaptic vesicles. *PNAS* **121**, e2409605121. https://doi.org/10.1073/pnas.2409605121.
72. Consortium, T.U., Bateman, A., Martin, M.-J., Orchard, S., Magrane, M., Ahmad, S., Alpi, E., Bowler-Barnett, E.H., Britto, R., Bye-A-Jee, H., Cukura, A., Denny, P., Dogan, T., Ebenezer, T., Fan, J., Garmiri, P., Gonzales, L.J. da C., Hatton-Ellis, E., Hussein, A., Ignatchenko, A., Insana, G., Ishtiaq, R., Joshi, V., Jyothi, D., Kandasaamy, S., Lock, A., Luciani, A., Lugaric, M., Luo, J., Lussi, Y., MacDougall, A., Madeira, F., Mahmoudy, M., Mishra, A., Moulang, K., Nightingale, A., Pundir, S., Qi, G., Raj, S., Raposo, P., Rice, D.L., Saidi, R., Santos, R., Speretta, E., Stephenson, J., Totoo, P., Turner, E., Tyagi, N., Vasudev, P., Warner, K., Watkins, X., Zaru, R., Zellner, H., Bridge, A.J., Aimo, L., Argoud-Puy, G., Auchincloss, A.H., Axelsen, K.B., Bansal, P., Baratin, D., Neto, T.M.B., Blatter, M.-C., Bolleman, J.T., Boutet, E., Breuza, L., Gil, B.C., Casals-Casas, C., Echioukh, K.C., Coudert, E., Cuche, B., de Castro, E., Estreicher, A., Famiglietti, M.L., Feuermann, M., Gasteiger, E., Gaudet, P., Gehant, S., Gerritsen, V., Gos, A., Gruaz, N., Hulo, C., Hyka-Nouspikel, N., Jungo, F., Kerhornou, A., Mercier, P.L., Lieberherr, D., Masson, P., Morgat, A., Muthukrishnan, V., Paesano, S., Pedruzzi, I., Pilbout, S., Pourcel, L., Poux, S., Pozzato, M., Pruess, M., Redaschi, N., Rivoire, C., Sigrist, C.J.A., Sonesson, K., Sundaram, S., Wu, C.H., Arighi, C.N., Arminski, L., Chen, C., Chen, Y., Huang, H., Laiho, K., McGarvey, P., Natale, D.A., Ross, K., Vinayaka, C.R., Wang, Q., Wang, Y., Zhang, J., (2022). UniProt: the Universal Protein Knowledgebase in 2023. *Nucleic Acids Res.* **51**, D523–D531. https://doi.org/10.1093/nar/gkac1052.
73. Piovesan, D., Conte, A.D., Clementel, D., Monzon, A.M., Bevilacqua, M., Aspromonte, M.C., Iserte, J.A., Orti, F.E., Marino-Buslje, Tosatto, S.C.E., (2022). MobiDB: 10 years of intrinsically disordered proteins. *Nucleic Acids Res.* **51**, D438–D444. https://doi.org/10.1093/nar/gkac1065.
74. Hubstenberger, A., Courel, M., Bénard, M., Souquere, S., Ernoult-Lange, M., Chouaib, R., Yi, Z., Morlot, J.-B., Munier, A., Fradet, M., Daunesse, M., Bertrand, E., Pierron, G., Mozziconacci, J., Kress, M., Weil, D., (2017). P-body purification reveals the condensation of repressed mRNA regulons. *Mol. Cell* **68**, 144–157.e5. https://doi.org/10.1016/j.molcel.2017.09.003.
75. Jain, S., Wheeler, J.R., Walters, R.W., Agrawal, A., Barsic, A., Parker, R., (2016). ATPase-modulated stress granules contain a diverse proteome and substructure. *Cell* **164**, 487–498. https://doi.org/10.1016/j.cell.2015.12.038.
76. Ward, J.H., (1963). Hierarchical grouping to optimize an objective function. *J. Am. Stat. Assoc.* **58**, 236. https://doi.org/10.2307/2282967.
77. Huerta-Cepas, J., Szklarczyk, D., Heller, D., Hernández-Plaza, A., Forslund, S.K., Cook, H., Mende, D.R., Letunic, I., Rattei, T., Jensen, L.J., von Mering, C., Bork, P., (2019). eggNOG 5.0: a hierarchical, functionally and phylogenetically annotated orthology resource based on 5090 organisms and 2502 viruses. *Nucleic Acids Res.* **47**, D309–D314. https://doi.org/10.1093/nar/gky1085.
78. Altschul, S.F., Gish, W., Miller, W., Myers, E.W., Lipman, D. J., (1990). Basic local alignment search tool. *J. Mol. Biol.* **215**, 403–410. https://doi.org/10.1016/s0022-2836(05)80360-2.
79. Edgar, R.C., (2004). MUSCLE: multiple sequence alignment with high accuracy and high throughput. *Nucleic Acids Res.* **32**, 1792–1797. https://doi.org/10.1093/nar/gkh340.
80. Waterhouse, A.M., Procter, J.B., Martin, D.M.A., Clamp, M., Barton, G.J., (2009). Jalview Version 2—a multiple sequence alignment editor and analysis workbench. *Bioinformatics* **25**, 1189–1191. https://doi.org/10.1093/bioinformatics/btp033.
81. Akshita, C., Christian, H., Aleksandr, K.A., Jakob, R., Linda, K., Luka, G., Cristina, R.-V., Emma, J.C., Jaqulin, W.N., Branislava, R., Eleonora, P., Sarah, K., Silvio, R.O., Helge, E., Jennifer, M.R., Dragomir, M., (2024). Condensates of synaptic vesicles and synapsin are molecular beacons for actin sequestering and polymerization. *BioRxiv*2024.07.19.604346. https://doi.org/10.1101/2024.07.19.604346.
82. Qin, D., Xia, Y., Whitesides, G.M., (2010). Soft lithography for micro- and nanoscale patterning. *Nature Protoc.* **5**, 491–502. https://doi.org/10.1038/nprot.2009.234.
83. Erkamp, N.A., Sneideris, T., Ausserwöger, H., Qian, D., Qamar, S., Nixon-Abell, J., George-Hyslop, P.S., Schmit, J.D., Weitz, D.A., Knowles, T.P.J., (2023). Spatially non-uniform condensates emerge from dynamically arrested phase separation. *Nature Commun.* **14**, 684. https://doi.org/10.1038/s41467-023-36059-1.
84. Ausserwöger, H., Scrutton, R., Sneideris, T., Fischer, C.M., Qian, D., de Csilléry, E., Saar, K.L., Białek, A.Z., Oeller, M., Krainer, G., Franzmann, T.M., Wittmann, S., Iglesias-Artola, J.M., Invernizzi, G., Hyman, A.A., Alberti, S., Lorenzen, N., Knowles, T.P.J., (2024). Biomolecular condensates sustain pH gradients at equilibrium driven by charge neutralisation. *BioRxiv*2024.05.23.595321. https://doi.org/10.1101/2024.05.23.595321.